AMERICAN SOCIETY FOR MICROBIOLOGY | Journal of Virology

The Presumed Polyomavirus Viroporin VP4 of Simian Virus 40 or Human BK Polyomavirus Is Not Required for Viral Progeny Release

Stian Henriksen,[a,b] Terkel Hansen,[c] Jack-Ansgar Bruun,[d] Christine Hanssen Rinaldo[a,e]

Department of Microbiology and Infection Control, University Hospital of North Norway, Tromsø, Norway[a]; Department of Clinical Medicine, UiT The Arctic University of Norway, Tromsø, Norway[b]; Department of Pharmacy, UiT The Arctic University of Norway, Tromsø, Norway[c]; Department of Medical Biology, UiT The Arctic University of Norway, Tromsø, Norway[d]; Metabolic and Renal Research Group, UiT The Arctic University of Norway, Tromsø, Norway[e]

ABSTRACT

The minor capsid protein of human BK polyomavirus (BKPyV), VP2, and its N-terminally truncated form, VP3, are both important for viral entry. The closely related simian virus 40 (SV40) reportedly produces an additional truncated form of VP2/3, denoted VP4, apparently functioning as a viroporin promoting progeny release. The VP4 open reading frame is conserved in some polyomaviruses, including BKPyV. In this study, we investigated the role of VP4 in BKPyV replication. By transfecting viral genomes into primary human renal proximal tubule epithelial cells, we demonstrated that unaltered BKPyV and mutants with start codon substitutions in VP4 (VP2M229I and VP2M229A) abolishing putative VP4 production were released at the same level to supernatants. However, during infection studies, VP2M229I and VP2M229A exhibited 90% and 65% reduced infectivity, respectively, indicating that isoleucine substitution inadvertently disrupted VP2/3 function to the detriment of viral entry, while inhibition of VP4 production during late infection was well tolerated. Unexpectedly, and similarly to BKPyV, wild-type SV40 and the corresponding VP4 start codon mutants (VP2M228I and VP2M228A) transfected into monkey kidney cell lines were also released at equal levels. Upon infection, only the VP2M228I mutant exhibited reduced infectivity, a 43% reduction, which also subsequently led to delayed host cell lysis. Mass spectrometry analysis of nuclear extracts from SV40-infected cells failed to identify VP4. Our results suggest that neither BKPyV nor SV40 require VP4 for progeny release. Moreover, our results reveal an important role in viral entry for the amino acid in VP2/VP3 unavoidably changed by VP4 start codon mutagenesis.

IMPORTANCE

Almost a decade ago, SV40 was reported to produce a late nonstructural protein, VP4, which forms pores in the nuclear membrane, facilitating progeny release. By performing transfection studies with unaltered BKPyV and SV40 and their respective VP4-deficient mutants, we found that VP4 is dispensable for progeny release, contrary to the original findings. However, infection studies demonstrated a counterintuitive reduction of infectivity of certain VP4-deficient mutants. In addition to the isoleucine-substituted SV40 mutant of the original study, we included alanine-substituted VP4-deficient mutants of BKPyV (VP2M229A) and SV40 (VP2M228A). These revealed that the reduction in infectivity was not caused by a lack of VP4 but rather depended on the identity of the single amino acid substituted within VP2/3 for VP4 start codon mutagenesis. Hopefully, our results will correct the longstanding misconception of VP4's role during infection and stimulate continued work on unraveling the mechanism for release of polyomavirus progeny.

Currently there are 13 known species of human polyomaviruses, and of these at least four are associated with diseases mainly affecting immunocompromised patients. BK polyomavirus (BKPyV) is the chief agent of polyomavirus-associated nephropathy (PyVAN) and polyomavirus-associated hemorrhagic cystitis (PyVHC), while JC polyomavirus (JCPyV) causes progressive multifocal leukoencephalopathy (PML). Merkel cell polyomavirus is associated with the rare but aggressive skin cancer Merkel cell carcinoma, and trichodysplasia spinulosa-associated polyomavirus causes the proliferative skin disease giving rise to its name. Although still not completely understood, a major component of the pathogenesis of PyVAN, PyVHC, and PML is thought to be the high-level lytic viral replication in renal tubular epithelial cells (1), bladder epithelial cells (2), and oligodendrocytes (3, 4), respectively.

Polyomaviruses are nonenveloped, spherical viruses with a diameter of about 45 nm (5, 6). The capsid has icosahedral symmetry, and the outer surface consists of the major capsid protein VP1 arranged in 72 pentamers. Inside the capsid, associated with the central cavity of each VP1 pentamer is one copy of either VP2 or VP3, the minor capsid proteins (7). These proteins bind the VP1 pentamers of the capsid to the circular double-stranded DNA genome. The genome can be functionally divided into an early region, late region, and noncoding control region (NCCR) (8). The early region encodes the regulatory large and small tumor antigens (LTag and sTag, respectively) and various truncated variants, while the late region encodes the capsid proteins VP1, VP2, and

Received 12 August 2016 Accepted 6 September 2016

Accepted manuscript posted online 14 September 2016

Citation Henriksen S, Hansen T, Bruun J-A, Rinaldo CH. 2016. The presumed polyomavirus viroporin VP4 of simian virus 40 or human BK polyomavirus is not required for viral progeny release. J Virol 90:10398–10413. doi:10.1128/JVI.01326-16.

Editor: L. Banks, International Centre for Genetic Engineering and Biotechnology

Address correspondence to Christine Hanssen Rinaldo, christine.rinaldo@unn.no.

Supplemental material for this article may be found at http://dx.doi.org/10.1128/JVI.01326-16.

VP3. In addition, the late region of JCPyV, BKPyV, and the closely related monkey polyomavirus, simian virus 40 (SV40), encodes agnoprotein, a nonstructural protein with incompletely characterized functions (8). In 2007, Daniels and colleagues reported that SV40 produces another late nonstructural protein, denoted VP4 (9). Interestingly, this small protein (13.9 kDa) was expressed 24 h after the other late proteins and is suggested to play a role in progeny release (9). The third genome region, the NCCR, contains the origin of replication, the early and late promoter, and enhancer sequences. During high-level virus replication, the NCCR is commonly rearranged. This frequently leads to an increased expression of LTag, which in turn causes enhanced viral replication (8, 10, 11).

Although the replication cycle of different polyomaviruses has been extensively studied, the process of progeny release is still unclear. Recently, several viruses have been proposed to produce viroporins, small hydrophobic proteins that oligomerize in host cell membranes, forming hydrophilic pores affecting several steps in the replication cycle, including progeny release (reviewed in reference 12). Four viroporins have been described for polyomaviruses: JCPyV agnoprotein (13), SV40 VP2 and VP3 (14), and SV40 VP4 (15, 16).

During SV40 replication, VP4 alone or in cooperation with VP2 and/or VP3 has been suggested to permeabilize the nuclear membrane, thereby disturbing the ionic homeostasis and enhancing progeny release (15, 17). The VP4 start codon, like that of VP3, lies within the sequence of VP2; thus, VP2, VP3, and VP4 share a C terminus. Polyclonal antibodies targeting the C-terminal part of VP2 or VP3 therefore should detect VP4 if it is produced, and this was in fact how SV40 VP4 expression was first demonstrated (9). Subsequent characterization of VP4 has been done mainly by biochemical approaches using recombinant VP4 (15–17).

Like SV40, the BKPyV genome has additional open reading frames (ORFs) downstream and in frame with the VP2 and VP3 ORFs, potentially encoding a BKPyV VP4 and two even smaller proteins, the putative VP5 and VP6, that all share a C terminus with VP2 and VP3 (Fig. 1A). The amino acid sequence of the C terminus contains important features, including a VP1-binding region, a DNA-binding region, and a nuclear localization signal (NLS) (Fig. 1A). Our initial aim was to investigate whether BKPyV-infected primary human renal proximal tubular epithelial cells (RPTECs) produce VP4 during a productive infection and to study a possible effect on virion release. Here, we report that BKPyV is not dependent on VP4 for effective progeny release. Instead, the two VP4-deficient BKPyV mutants were found to be defective in entry events, and this phenotype was dependent on the identity of the amino acid in VP2 and/or VP3 unavoidably changed during the substitution of the initial methionine of VP4. To investigate the effect on infectivity for SV40 VP4-deficient mutants, we repeated our experiments using SV40 as in the original VP4 report. Surprisingly, we obtained results similar to those for BKPyV. SV40 progeny release did not depend on VP4 expression, and entry was affected by one amino acid change in VP2 and/or VP3. Moreover, we were not able to detect VP4 in SV40-infected cells despite searches using tandem mass spectrometry (MS/MS). Our results cast doubt on the suggested role of VP4 in the polyomavirus replication cycle.

MATERIALS AND METHODS

Viruses, plasmids, and mutagenesis. All BKPyV experiments were performed with BKPyV Dunlop (ATCC 45025) (wild type [WT]) or BKPyV WW (WW WT) and virus with mutation of the start codon of VP2, VP3, VP4, or both VP2 and VP3 (Table 1). All SV40 experiments were performed with strain 776 and virus with start codon mutations of VP4 (Table 1). All mutants were created by long PCR of pBKV (34-2) (ATCC 45025) (18), pBKV WWT (19), or pWTSV40 JL (20) using overlapping primers that targeted the ATG start codon (Table 1) and the high-fidelity Phusion polymerase (M0530S; New England BioLabs) according to the manufacturer's instructions as previously described (21). Sanger sequencing confirmed successful mutagenesis. BKPyV VP1, VP3, and VP4 expression plasmids with N-terminal enhanced green fluorescent protein (eGFP) tags were created by gateway cloning using a pDEST-EGFP-C1 destination vector (22) kindly provided by Ole Morten Seternes, UiT The Arctic University of Norway. Codon-optimized SV40 VP4 expression plasmid with C-terminal eGFP tag was codon optimized for human cells by GenScript.

Cells. The African green monkey kidney cell lines Vero (ATCC CCL-81) and BS-C-1 (ATCC CCL-26) were cultured in Dulbecco's modified Eagle's medium (D5671; Sigma-Aldrich) supplemented with 10% fetal bovine serum (FBS) and 1× GlutaMAX-I (no. 35050; Thermo Fisher Scientific). The African green monkey kidney cell line CV-1 (ATCC CCL-70) and the SV40-LTag-transformed COS-7 (ATCC CRL-1651) cells were cultured in Dulbecco's modified Eagle's medium supplemented with 5% FBS and 1× GlutaMAX-I. HeLa cells (ATCC CCL-2) were cultured in modified Eagle's medium (M2279; Sigma-Aldrich) supplemented with 10% FBS and 1× GlutaMAX-I. Primary human renal proximal tubular epithelial cells (RPTECs; ScienCell Research Laboratories) were cultured in renal epithelial growth medium (REGM; Lonza) containing 0.5% FBS and used at passage 4. All cells were cultivated in a humidified 5% CO_2 incubator at 37°C.

Transfections. Transfection of RPTECs was performed by electroporation using the Neon transfection system (Thermo Fisher Scientific). In short, 0.1 μg of BamHI-linearized and ligated plasmid was transfected into 2.5×10^4 cells, and electroporation was performed in 10-μl electroporation tips and with 1 pulse at 1,400 V and 20-ms pulse width. Transfected cells were seeded in plates with REGM without antibiotics. The day after transfection, the cell medium was replaced with fresh complete REGM. Transfection of CV-1, BS-C-1, Vero, and HeLa cells was performed with Lipofectamine 2000 (Thermo Fisher Scientific) according to the manufacturer's instructions. In short, for transfection in wells in a 48-well plate, 0.1 μg linearized and ligated plasmid was mixed with the empty plasmid vector pUC19 to get a final DNA concentration of 0.5 μg per transfection. The ratio of DNA (micrograms) to Lipofectamine 2000 (microliters) was 1:2 for CV-1 and Vero cells, 1:1.5 for BS-C-1 cells, and 1:3 for HeLa cells. The cell medium containing the transfection mix was removed and fresh medium was added at 4 to 6 h posttransfection (hpt). For mock transfections, 0.5 μg pUC19 was used alone.

Viral infections. Supernatants from BKPyV-transfected RPTECs and Vero cells or SV40-transfected CV-1 and BS-C-1 cells were diluted 1:2 in fresh complete medium and used to infect RPTECs and CV-1 cells, respectively. All infections were carried out for 2 h before the infectious inoculum was removed, cells were washed once with 1× phosphate-buffered saline (PBS), and complete medium was added.

Immunofluorescence staining, microscopy, and digital image processing. Infected and transfected cell monolayers were fixed with 4% paraformaldehyde in PBS for 10 min and permeabilized with 100% methanol for 10 min, and then immunofluorescence was performed as described earlier (23). The primary antibodies used were mouse monoclonal SV40 LTag (Ab-2; 1:100; Calbiochem), SV40 LTag (Pab419; 1:100; Santa Cruz Biotechnology), BKPyV VP1 (4942; 2.8 μg/ml; Virostat Inc.), and rabbit polyclonal antiserum directed against BKPyV agnoprotein (1:1,000) (24), BKPyV VP1 (1:1,000) (25), SV40 VP1 (Ab53977; 1:1,000, Abcam), and SV40 VP2/3 (Ab53983; 1:1,000; Abcam). The secondary

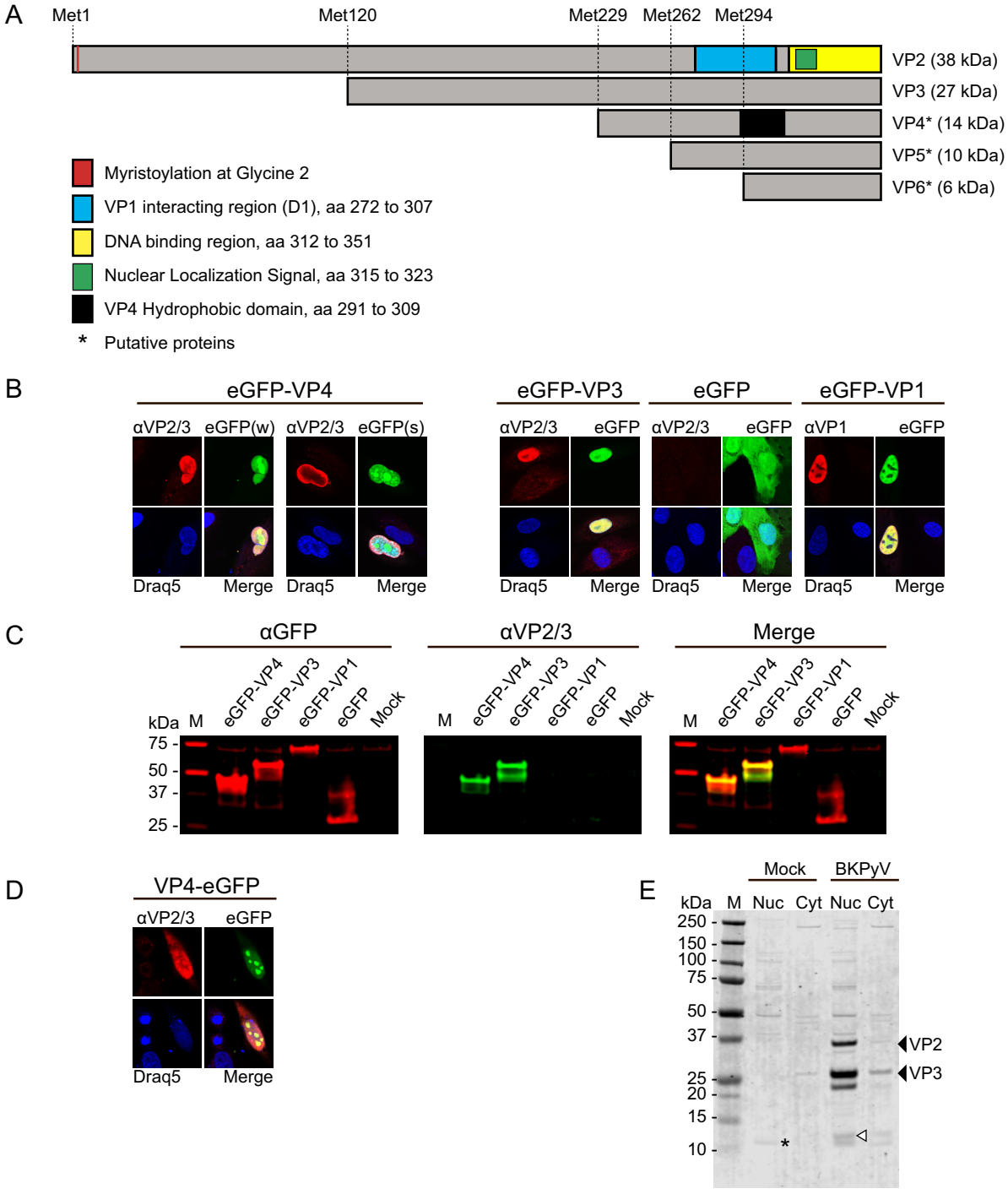

FIG 1 BKPyV minor capsid proteins are recognized by SV40 VP2/3 antiserum. (A) Schematic overview of BKPyV minor capsid protein VP2 and its confirmed and putative truncated variants. Annotated regions and motifs are derived from the UniProtKB database, accession numbers P03093 and P03094, and the VP4 hydrophobic domain is annotated by similarity to SV40 VP4. (B) Immunofluorescence labeling of RPTECs at 1 dpt with the eGFP-VP4 expression plasmid, using the SV40 VP2/3 antisera (red) and the DNA stain Draq5 (blue). The level of eGFP expression is indicated in parentheses as weak (w) or strong (s). As a positive and negative control for the SV40 VP2/3 antiserum, RPTECs were transfected with eGFP-VP3 and eGFP, respectively. In addition, cells were transfected with eGFP-VP1 plasmid and immunofluorescence labeling was performed using the BKPyV VP1 antisera (red). Images were acquired by confocal microscopy with a 40× objective and with a 2× zoom. (C) Western blot of HeLa cell lysate harvested at 1 dpt with the indicated expression plasmids. The membrane was probed with a GFP antibody (red) and the SV40 VP2/3 antisera (green). M, molecular mass marker. (D) Immunofluorescence labeling of HeLa cells at 1 dpt with the SV40 VP4-eGFP expression plasmid, using the SV40 VP2/3 antisera (red) and the DNA stain Draq5 (blue). VP4-eGFP is shown in green. Images were acquired by confocal microscopy with a 40× objective and a 2× zoom. (E) Western blot of nuclear and cytoplasmic cell fractions of mock-infected and BKPyV-infected RPTECs harvested at 3 dpi. The membrane was probed with the SV40 VP2/3 antisera. The empty arrowhead indicates a band with the expected size of BKPyV VP4, and the asterisk indicates a nonspecific band in the mock-infected nuclear fraction. Nuc, nuclear fraction; Cyt, cytoplasmic fraction.

TABLE 1 Mutated genomes and mutagenesis primers

Original genome (in plasmid form), mutated genome, and primer designation	Mutagenesis primer sequence (5′ to 3′)	Introduced change in VP2[a]	Start codon targeted
BKPyV Dunlop (pBKV34-2)			
VP2M229I			
1F	GCC CTC AAT AGT TAG ACA AGT AGC TGA AAG	aa 229	Putative VP4
1R	AAC TAT TGA GGG CCT AAT AGG GGA AAG AT	ATG to ATA (Met to Ile)	
VP2M229A			
2F	GCC CTC AGC CGT TAG ACA AGT AGC TGA AAG	aa 229	Putative VP4
2R	AAC GGC TGA GGG CCT AAT AGG GGA AAG AT	ATG to GCC (Met to Ala)	
ΔVP2			
3F	AGG TTC ATA GGT GCT GCT CTA GCA C	aa 1	VP2
3R	GCA GCA CCT ATG AAC CTG GAA ATA C	ATG to ATA (Met to Ile)	
ΔVP3			
4F	GGC ATA GCT TTG GAA TTG TTT AAC CC	aa 120	VP3
4R	AAA GCT ATG CCT GAT TGC TGA TAG AG	ATG to ATA (Met to Ile)	
BKPyV WW (pBKV WWT)			
WW VP2M229I			
1F	GCC CTC AAT AGT TAG ACA AGT AGC TGA AAG	aa 229	Putative VP4
1R	AAC TAT TGA GGG CCT AAT AGG GGA AAG AT	ATG to ATA (Met to Ile)	
SV40 776 (pWTSV40)			
VP2M228I			
1F	GCC TAC AAT AGT GAG ACA AGT AGC CAA CAG	aa 228	Putative VP4
1R	CAC TAT TGT AGG CCT AAT GGG AGA CAA AG	ATG to ATA (Met to Ile)	
VP2M228A			
2F	GCC TAC AGC CGT GAG ACA AGT AGC CAA CAG	aa 228	Putative VP4
2R	CAC GGC TGT AGG CCT AAT GGG AGA CAA AG	ATG to ATA (Met to Ile)	

[a] aa, amino acid.

antibodies were anti-mouse conjugated with Alexa Fluor 568 and anti-rabbit conjugated with Alexa Fluor 488 or with Alexa Fluor 568 (1:500; Molecular Probes). Nuclear DNA was labeled with Draq5 (1:1,000; Biostatus). Images were captured and processed using a Nikon TE2000 microscope and NIS Elements basic research software, version 4 (Nikon Corporation), or a Zeiss LSM 780 confocal microscope and ZEN 2 software.

Quantification of virus protein-expressing cells. To quantify the number of VP1-, LTag-, and agnoprotein-expressing cells in immunofluorescently stained cells, the object count feature in NIS Elements software was used. Each experiment was done in duplicate wells, and for each well 5 images were acquired using a 10× objective. For each well, approximately 3,000 to 5,000 Draq5-positive cells were analyzed for virus protein expression, except for infection with BKPyV WW, where all agnoprotein-expressing cells were counted.

Quantification of extracellular encapsidated BKPyV and SV40 DNA. Encapsidated extracellular BKPyV and SV40 DNA was quantified by quantitative PCR (qPCR) of DNase I-treated supernatants using primers and probes targeting the BKPyV and SV40 LTag gene, respectively (26, 27). The DNase I treatment was performed directly on the supernatants using the Turbo DNA-free kit (AM1907; Thermo Fisher Scientific) according to the manufacturer's instructions. After DNase I removal, the supernatants were diluted in molecular-grade water (1:100; Lonza) and boiled for 5 min before 5 μl was used as a template for a 25-μl qPCR mixture. Each sample was analyzed in triplicate.

Virus pelleting. Supernatants from BKPyV-transfected RPTECs or SV40-transfected CV-1 cells were collected 2 dpt, clarified by low-speed centrifugation at 10,000 × *g* for 30 min at 4°C, and then ultracentrifuged in Beckmann ultraclear tubes in an SW 50.1 rotor at 30,000 rpm for 1 h at 4°C. The supernatant was removed and the pellet dissolved in 100 μl 10 mM Tris-HCl, 1 mM $CaCl_2$, pH 7.4, and then subjected to protein gel electrophoresis and Western blotting.

Protein gel electrophoresis and Western blotting. Cells were lysed in radioimmunoprecipitation assay (RIPA) buffer (21) with protease inhibitor (cOmplete, mini, EDTA-free; Roche) or fractionated into nuclear and cytoplasmic fractions using a nuclear extract kit (40010; Active Motif) at the indicated time points. When required, total protein concentration was measured using the EZQ protein quantitation kit (Thermo Fisher Scientific) according to the manufacturer's instructions. The lysates and fractions were stored at −70°C until separation on a NuPAGE 4 to 12% Bis-Tris gel (Thermo Fisher Scientific) and blotting onto a polyvinyl difluoride membrane (Thermo Fisher Scientific). The membrane was blocked with Odyssey blocking buffer (LI-COR Biosciences) and incubated with the following primary antibodies: rabbit polyclonal antiserum directed against BKPyV VP1 (1:10,000) (25), SV40 VP1 (Ab53977; 1:10,000; Abcam), and SV40 VP2/3 (Ab53983; 1:10,000; Abcam) and mouse monoclonal antibody directed against glyceraldehyde-3-phosphate dehydrogenase (GAPDH) (Ab8245; 1:5,000; Abcam) or GFP tag mouse monoclonal antibody (GF28R; 1:1,000; Médimabs; a kind gift from Kenneth Bowitz Larsen at the Advanced Microscopy Core Facility, UiT The Arctic University of Norway). The secondary antibodies were anti-rabbit and anti-mouse infrared dye-labeled antibodies (IRDye 680LT goat anti-mouse [1:20,000] and IRDye 800CW goat anti-rabbit [1:15,000]; LI-COR Biosciences). The Odyssey CLx imaging system (LI-COR Biosciences) and Image Studio Lite (version 5.2) were used for detection and data acquisition.

Viability assays. The electrical impedance of mock-transfected, SV40 WT-transfected, and VP4-deficient mutant-transfected CV-1 cells was measured using E plates (E-Plate View; ACEA Biosciences) and the xCELLigence system (ACEA Biosciences). The background impedance of the wells was measured after addition of 100 μl complete cell medium to each well. At 6 hpt, 100 μl of transfected CV-1 cells was added into the wells. Each transfection was performed in quadruplicate. Impedance was measured every 10 min for the first 60 h and then every 30 min up to 120 hpt, when cells were fixed for immunofluorescence staining. Impedance was expressed as an arbitrary unit called the cell index, and the cell index for all wells was set to zero at 12 hpt. The impedance of mock-transfected

cells was set as a baseline, and the impedance of the other cells was normalized to this. One representative experiment is shown.

Time-lapse microscopy. For continuous microscopic monitoring of mock-, SV40 WT-, and VP4-deficient mutant-infected CV-1 cells, a Nikon Biostation (Nikon Corporation) was used. Cells were seeded at 60,000 cells/well in Hi-Q4 culture dishes (Ibidi) in 500 μl DMEM with 5% FBS and a 1:1,000 dilution of the green cyanine dye from the CellTox green cytotoxicity assay (Promega). Pictures were taken at 5 points in each well every 15 min from 6 h postinfection (hpi).

Immunoprecipitation. Immunoprecipitation was performed using SV40 VP2/3 antisera (Ab53983; Abcam) and capturing using protein A magnetic Sepharose (GE Healthcare). For each immunoprecipitation, nuclear extracts were harvested at 3 to 6 days postinfection (dpi) from SV40-infected CV-1 cells grown to confluence on an area of approximately 87.5 cm^2. In short, 10 μl of the SV40 antisera mixed with 50 μl nuclear extracts diluted in 250 μl Tris-buffered saline (TBS; 50 mM Tris, 150 mM NaCl, pH 7.5) was incubated for 16 h at 4°C with slow end-over-end mixing. The antibody-antigen complex was captured by the addition of 20 μl protein A magnetic Sepharose followed by incubation for 2 h at room temperature with slow end-over-end mixing. The Sepharose was then washed thrice with 500 μl TBS. The antibody-antigen complex was eluted in LDS sample buffer (Thermo Fisher Scientific) containing sample reducing agent (Thermo Fisher Scientific) by heating to 70°C for 10 min and was separated on an SDS-PAGE gel.

Dimethyl labeling of proteins. Dimethyl labeling of free N-terminal ends and lysine residues of proteins in nuclear extracts from SV40-infected CV-1 cells was performed as previously described (28). In brief, freshly isolated nuclear extracts were incubated for 2 h at 37°C with gentle agitation in a labeling buffer consisting of 20 mM formaldehyde, 40 mM sodium cyanoborohydride, and 200 mM HEPES at pH 8.0. The excess formaldehyde was quenched by addition of glycine to a final concentration of 60 mM, followed by incubation for 10 min at room temperature. The samples were then treated with 130 mM hydroxylamine hydrochloride for 15 min at room temperature before adding LDS sample buffer and subsequent SDS-PAGE gel separation.

MS. Analysis using liquid chromatography-tandem mass spectrometry (LC-MS/MS) was performed at the Tromsø University Proteomics Platform from gel slices of Coomassie-stained (SimplyBlue SafeStain; Thermo Fisher Scientific) SDS-PAGE gels. Gel slices were subjected to in-gel reduction, alkylation, and protease digestion with 6 ng/μl trypsin (V5111; Promega) or 6 ng/μl chymotrypsin (V1062; Promega) (29). OMIX C_{18} tips (Varian, Inc., Palo Alto, CA, USA) were used for sample cleanup and concentration. Peptide mixtures containing 0.1% formic acid were loaded onto a Thermo Fisher Scientific EASY-nLC 1000 system and EASY-spray column (C_{18}; 2 μm; 100 Å; 50 μm; 50 cm). Peptides were fractionated using a 2 to 100% acetonitrile gradient in 0.1% formic acid over 50 min at a flow rate of 200 nl/min. The separated peptides were analyzed using a Thermo Scientific Q-Exactive mass spectrometer.

To search for N-terminal VP4 peptides, an inclusion list was used. This list contained 2+ and 3+ *m/z* for the dimethyl-labeled (+28 amu), chymotrypsin-derived N-terminal peptide (MVRQVANREGLQISF) with and without methionine. The retention time determined for the positive control (±1 min) was included in the inclusion list. When idle, data were collected in data-dependent mode using a Top10 method. The raw data were processed using PEAKS Studio 7 software (v. 7.0; Bioinformatics Solutions, Canada). Fragmentation spectra were searched in PEAKS against a combined *Chlorocebus* and SV40 proteome.

RESULTS

BKPyV-infected RPTECs contain a protein of mass similar to that of SV40 VP4. In the original SV40 VP4 report, the putative 13.9-kDa protein was detected by Western blotting of nuclear extracts from SV40-infected BS-C-1 cells using a polyclonal antiserum directed against SV40 VP2/3 (9). Similar to SV40 VP4, the potential BKPyV VP4 protein has a C-terminal NLS (Fig. 1A) and would also be expected to localize to the nucleus. We first investigated if a polyclonal SV40 VP2/3 antiserum raised against the full-length SV40 VP3 protein but previously found to recognize BKPyV VP2 and VP3 (S. Henriksen and C. H. Rinaldo, unpublished observations) would recognize a recombinant BKPyV VP4 protein with an N-terminal eGFP tag, here denoted eGFP-VP4. The eGFP-VP4 expression vector was transfected into RPTECs. As controls, the same expression vector encoding eGFP-VP3, eGFP alone, or eGFP-VP1 was used. At 24 hpt, cells were fixed and immunofluorescence staining with the SV40 VP2/3 antiserum or with BKPyV VP1 antiserum was performed. Confocal microscopy confirmed that the eGFP-VP4 proteins were localized in the nucleus and verified that they could be recognized by the SV40 VP2/3 antiserum (Fig. 1B). Interestingly, in cells with weak eGFP-VP4 signal, the eGFP-VP4 proteins formed large nuclear inclusions that were also labeled by the SV40 VP2/3 antiserum (Fig. 1B, left), while in cells with a stronger eGFP-VP4 signal, the immunostaining was mainly restricted to the nuclear rim, and the inclusions were smaller and colocalized with the speckled DNA staining (Fig. 1B, right). The DNA staining pattern suggests DNA fragmentation in cells with high eGFP-VP4 expression. In the control transfections, eGFP-VP3 and eGFP-VP1 localized to the nucleus while eGFP alone was present in both the nucleus and the cytoplasm (Fig. 1B). Of note, VP1 contains a different NLS than VP2/3/4. In the control transfections, no nuclear inclusion bodies or speckled DNA staining was seen, and in contrast to the eGFP-VP4-expressing cells, eGFP-VP3- and eGFP-VP1-expressing cells demonstrated a high degree of colocalization of the immunostaining and the eGFP signal.

To confirm that the SV40 VP2/3 antiserum would also recognize denatured BKPyV VP4, we performed SDS-PAGE followed by Western blotting of cell lysates from CV-1 cells transfected with the eGFP-VP4 expression vector or expression vectors encoding eGFP-VP3, eGFP-VP1, or eGFP alone. The Western blot, labeled with a monoclonal GFP antibody (red) and the SV40 VP2/3 antiserum (green), demonstrated bands with the expected molecular mass of the recombinant proteins (eGFP-VP4, ~42 kDa; eGFP-VP3, ~55 kDa; eGFP-VP1, ~68 kDa; and eGFP, ~28 kDa) (Fig. 1C). Interestingly, in contrast to the eGFP-VP1 lysate, both the eGFP-VP4 and eGFP-VP3 lysate gave rise to additional bands that migrated faster than expected and were labeled with both GFP and SV40 VP2/3 antisera, indicating that the C-terminal part of the recombinant proteins was prone to degradation or proteolysis.

Several attempts on expressing and detecting untagged BKPyV VP4 or BKPyV VP4 with a small C-terminal tag, V5-tag, were unsuccessful. However, when the codons of the SV40 VP4 gene were optimized to resemble human codon usage, we were able to produce VP4 with a C-terminal eGFP tag, VP4-eGFP, by transfection of HeLa cells. VP4-eGFP was mainly localized to the nucleus, but some cytoplasmic staining also was seen (Fig. 1D), possibly due to degradation and proteolysis (results not shown).

Together these results suggest that BKPyV VP4, if expressed, would localize to the nucleus and could be detected by the SV40 VP2/3 antiserum.

We next wanted to investigate the potential expression of BKPyV VP4 during infection of RPTECs, the natural host cells for BKPyV during latency and disease. RPTECs were infected with BKPyV Dunlop and at 72 hpi, corresponding to one complete replication cycle (30, 31), cells were harvested and separated into cytoplasmic and nuclear fractions before SDS-PAGE and Western

blotting with the SV40 VP2/3 antiserum was performed. Cytoplasmic and nuclear fractions from mock-infected cells were used as controls. As expected, a strong expression of proteins with the predicted size of VP2 and VP3 was observed only in nuclear extracts from BKPyV-infected cells (Fig. 1E). In addition, a slightly faster migrating band was observed below VP2 and VP3. Based on the results shown in Fig. 1C, this is probably protolysed VP2 and VP3, respectively. Of note, a weak band with the predicted size of VP4 was seen, suggesting that BKPyV expresses VP4. Similar to the original SV40 VP4 report (9), we also detected a faint band with a lower molecular mass which could correspond to a protein made from one of the two downstream ORFs (Fig. 1A). A weak band between 10 and 15 kDa was also noted in mock-infected cells. Moreover, for both mock-infected and BKPyV-infected cells, several bands with molecular masses higher than 37 kDa were observed, possibly due to unspecific binding of the SV40 VP2/VP3 antiserum.

We conclude that BKPyV might express a VP4 protein and that this probably is located in the nucleus. A novel truncated form of VP4, denoted VP5 or VP6, may be expressed as well.

BKPyV strain Dunlop does not require the nonstructural protein VP4 or minor capsid proteins VP2/VP3 for progeny release, but VP2-, VP3-, and VP4-deficient mutants show reduced infectivity compared to the WT strain. In the original VP4 report (9), a VP4-defective mutant, termed VP2M228I, was created by changing the start codon from ATG (methionine) to ATA (isoleucine), thereby unavoidably introducing one point mutation into both VP2 and VP3. In order to study the function of the putative BKPyV VP4 protein, we used site-directed mutagenesis to create a homologous VP4-deficient BKPyV mutant, VP2M229I. To reduce the possibility of revertants and to explore the tolerance of mutations for VP2/3 functions, we generated a second mutant, VP2M229A, by changing the start codon to GCC (alanine). As controls, we also made mutants with start codon substitutions (methionine to isoleucine) in VP2 (ΔVP2), in VP3 (ΔVP3), and in both VP2 and VP3 (ΔVP2/ΔVP3).

In order to test protein expression directed from the different recombinant viruses, we transfected equal amounts of the mutated genomes into RPTECs and harvested cell lysates for Western blot analysis at 2 days posttransfection (dpt) (Fig. 2A). SDS-PAGE followed by Western blotting with the SV40 VP2/3 antiserum in combination with the BKPyV VP1 antiserum demonstrated that cells transfected with the VP4-deficient mutants produced VP2 and VP3. The VP2-deficient mutant and the VP3-deficient mutant only produced VP3 or VP2, respectively, while no minor capsid proteins were detected in cells transfected with the VP2/3-deficient mutant. Moreover, all mutants produced VP1 at levels comparable to the WT virus.

In order to investigate the release of viral progeny after about one replication cycle, we again transfected RPTECs with equal amounts of the WT and the mutated genomes and harvested the supernatants at 3 dpt for quantification of encapsidated viral genomes (i.e., DNase I-protected BKPyV DNA) by qPCR. The DNase I digestion step reduced the amount of nonencapsidated viral DNA originating from the transfection (input at 1 dpt) to about 10^6 genomic equivalents (GEq)/ml (Fig. 2B). The results showed a >2-log increase in encapsidated BKPyV DNA in supernatants from cells transfected with BKPyV WT 3 dpt (Fig. 2B). Surprisingly, given the suspected role of VP4 in viral release, both VP4-deficient mutants were released at a similar level (Fig. 2B), suggesting that BKPyV does not require VP4 for viral progeny release. Interestingly, a similar release was also found for virions without VP2 or VP3 or without both VP2 and VP3 (Fig. 2B). To ensure that this unaffected release was not due to the host cells chosen, the transfections were repeated in Vero cells. However, the results were similar to what we found in RPTECs (results not shown). To confirm that cells transfected with the different mutants actually released virions, Vero cells were transfected with the same constructs and supernatants harvested 2 dpt. Virions were pelleted by ultracentrifugation, and a portion of this was analyzed by SDS-PAGE and Western blotting, using the same combination of the VP2/3 and VP1 antisera as before. Based on the VP1 band, the result confirmed a similar amount of extracellular virus for all mutants (Fig. 2C). In addition, the results confirmed the absence and presence of VP2 and VP3 in the mutants.

Since we did not find that the absence of VP4 affected BKPyV release when the entry events were bypassed by DNA transfection, we next investigated if the early events in the replication cycle were affected by the lack of VP4. Supernatants harvested from RPTECs 3 dpt were used to infect new RPTECs, and immunofluorescent staining with a combination of antisera directed against BKPyV agnoprotein and a monoclonal antibody directed against LTag was performed at 3 dpi. Immunofluorescence microscopy revealed that 27% and 11% of cells infected with the WT virus supernatant expressed LTag and agno protein, respectively (Fig. 2D). Compared to WT virus, both of the VP4-deficient mutants displayed reduced infectivity. Interestingly, the VP2M229A mutation was better tolerated by the virus, giving only a 65% overall reduction, compared with the 90% reduction of the VP2M229I mutation. If the reduced infectivity was caused by the lack of VP4, we would have expected a similar infectivity of the two VP4-deficient mutants. Since this was not the case, the results suggest that at least part of the observed reduction in infectivity was due to the simultaneous introduction of one amino acid change in the VP2 and/or VP3 sequence that was unavoidably created during VP4 start codon mutation.

The importance of the minor capsid proteins in infection was further emphasized by the fact that that mutants deficient in either VP2 or VP3 or both VP2 and VP3 were almost noninfectious, causing a more than 99% reduction of LTag and agno protein expressing cells compared to the WT strain (Fig. 2D).

We conclude that VP4 has no measurable role in BKPyV release in cell culture. Not surprisingly, the presumed late and nonstructural VP4 is not required for the early steps of the viral replication cycle. However, what seems clear is that amino acid 229 in VP2 and/or amino acid 110 in VP3, both overlapping the VP4 start codon, play important roles in the early steps of the BKPyV replication cycle.

The archetype strain of BKPyV, WW, does not require VP4 for efficient progeny release, but a mutation of VP2 amino acid 229 and/or VP3 amino acid 110 causes reduced infectivity compared to the WT strain. In the above-described experiments, we used the BKPyV strain Dunlop, which has a high replication capacity in both primary human RPTECs and in various cell lines. In contrast to this, the BKPyV archetype strain WW, usually found in urine of healthy individuals, has a low replication capacity both *in vivo* and in cell culture (10, 11). Although the low replication capacity is mainly caused by a low level of early gene expression and DNA replication, the mechanism for virion release might also differ. We therefore investigated if the WW strain required the

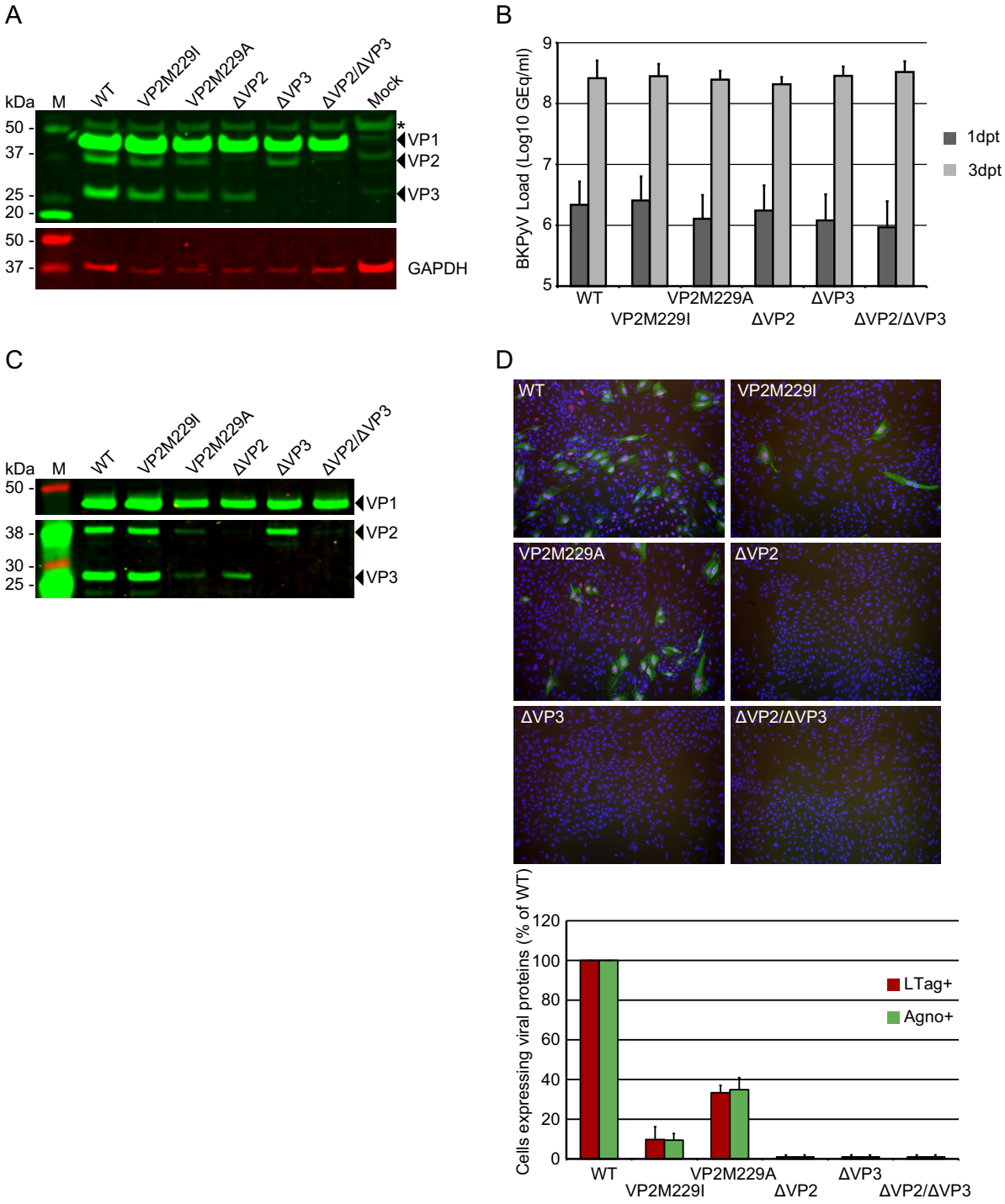

FIG 2 BKPyV VP4 is not required for viral progeny release, but VP4 start codon substitution affects infectivity. (A) Western blot of RPTEC cell lysates harvested at 2 dpt with the indicated BKPyV genomes. The membrane was probed with rabbit BKPyV VP1 antisera (green) and rabbit SV40 VP2/3 antisera (green). Mouse GAPDH antibody was used as a loading control (red). The asterisk indicates binding to a nonspecific cellular protein by the VP1 or VP2/3 antisera. M, molecular mass marker. (B) BKPyV load in DNase I-treated supernatants from RPTECs at 1 and 3 dpt, determined by real-time quantitative PCR and presented as GEq/ml. The figure represents data from three independent experiments, each performed in duplicate wells, and the error bars indicate the standard deviations. (C) Western blot of capsid proteins pelleted by ultracentrifugation from Vero cell supernatants harvested 3 dpt. A volume corresponding to 400 μl supernatant was loaded on the gel. The membrane was probed with rabbit BKPyV VP1 antisera (upper) and rabbit SV40 VP2/3 antisera (lower). The signal intensity in the lower panel was increased for better visualization of the VP2 and VP3 proteins. (D) Immunofluorescence staining of RPTECs at 3 dpi with the indicated BKPyV variants at similar BKPyV load (approximately 8 $\log_{10}$ GEq/ml), using the rabbit agno antisera (green) and the mouse monoclonal LTag antibody (Ab-2; red). Representative images of the immunofluorescence staining are shown in the upper panel, and quantification in relation to the WT infection is displayed in the graph in the lower panel. Each experiment was done in duplicate and repeated twice. Approximately 3,000 to 5,000 Draq5-positive cells per well were analyzed for virus protein expression.

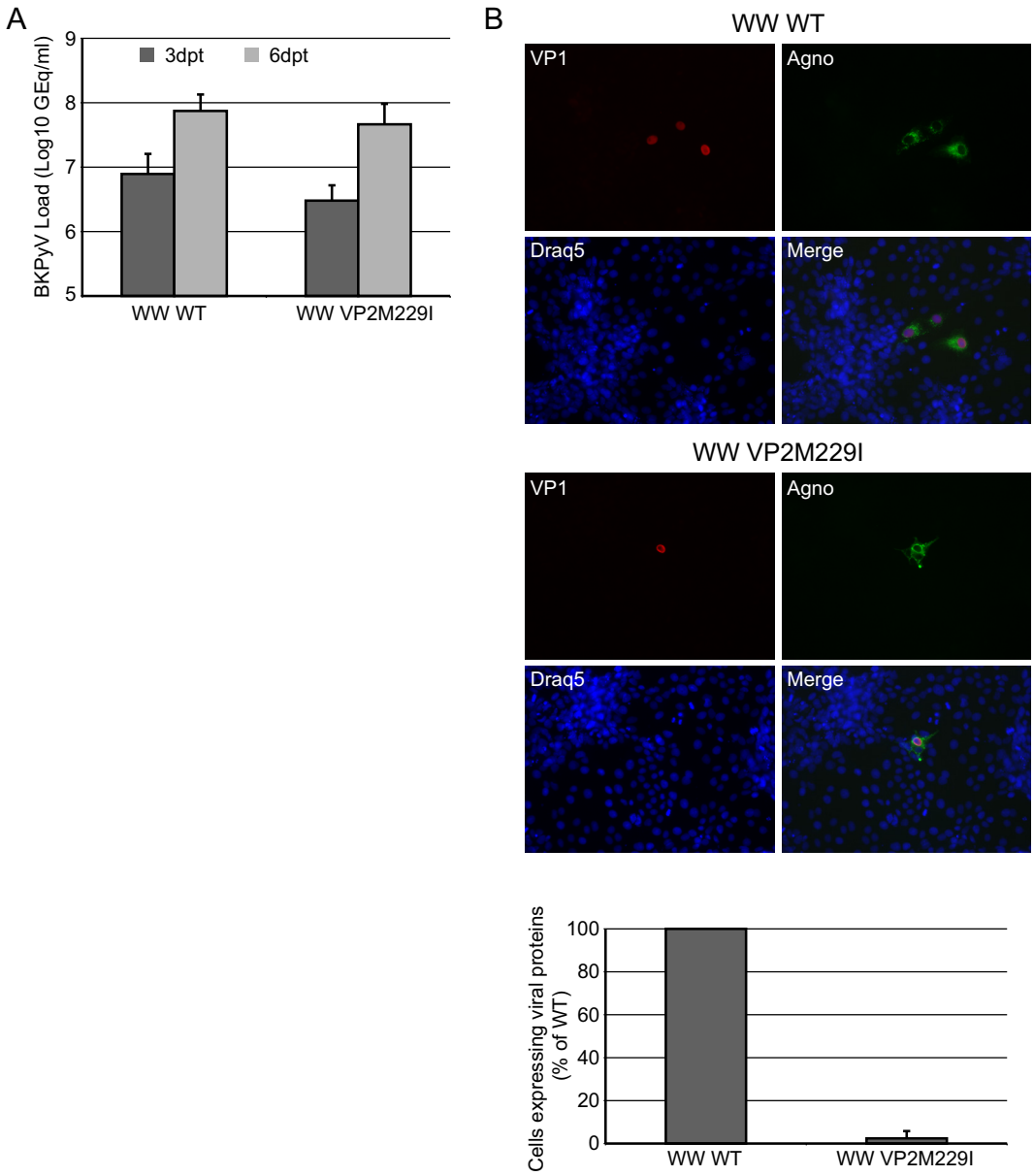

FIG 3 BKPyV VP4 is not required for viral progeny release of the WW strain, but the VP4 start codon substitution M229I affects infectivity. (A) BKPyV load in DNase I-treated supernatants from RPTECs at 3 and 6 dpt, determined by real-time quantitative PCR and presented as GEq/ml. The figure represents data from two independent experiments, each performed in duplicate wells, and the error bars indicate the standard deviations. (B) Immunofluorescence staining of COS-7 cells 4 dpi with BKPyV WW WT and BKPyV WW VP2M229I at similar viral loads (approximately 8 $\log_{10}$ GEq/ml) using a BKPyV VP1 antibody (red) and the agno antisera (green). Representative images of the immunofluorescence staining are shown in the upper panels, and quantification in relation to WT infection is displayed in the graph in the lower panel. Each experiment was performed twice in duplicate wells. All agno-positive cells present in 0.75-cm^2 wells were counted.

putative VP4 protein for viral progeny release. Using the same experimental approach as that for the Dunlop strain, we created a WW strain with a VP4 start codon mutation, WW VP2M229I, and transfected both the wild-type WW strain (WW WT) and the mutant into RPTECs. As expected, qPCR of the DNase I-treated supernatants 3 dpt confirmed that the infection with WW WT progressed much slower than that with the Dunlop strain. The DNA load was about 10^7 GEq/ml (Fig. 3A), which was about 1 log less than that for Dunlop (Fig. 2B), but increased to similar levels by 6 dpt (Fig. 3A). Importantly, the VP4-deficient mutant was released at a similar level (Fig. 3A). These results suggest that, similar to BKPyV Dunlop, archetypal BKPyV does not require VP4 for progeny release.

To investigate the effects of the mutation on early events, supernatants from 6 dpt were used to infect RPTECs, and this was followed by immunofluorescent staining at 3 dpi. Although we observed fewer infected cells in RPTECs inoculated with supernatants from the VP4-deficient mutant than cells inoculated with WW WT supernatants, the overall low number of infected cells made it difficult to determine if there was a significant difference (results not shown). We therefore

infected COS-7 cells, a cell line that constitutively produces SV40 LTag. By doing this, we were able to slightly increase the number of WW WT-infected cells (Fig. 3B). Compared to the WT, the infectivity of the mutant was 98% reduced (Fig. 3B).

We conclude that VP4 is not required for WW release. Taken together with our earlier results, these results suggest that the alteration of amino acid 229 in VP2 and/or amino acid 110 in VP3, from methionine to isoleucine, reduces infectivity of BKPyV WW.

SV40 infection in various cell lines does not require VP4 for efficient progeny release; however, the SV40 VP4-deficient mutant VP2M228I, but not VP2M228A, show reduced infectivity compared to SV40 WT. Given our surprising results for the BKPyV VP4-deficient mutants, we decided to apply our methods using SV40 WT and VP4-deficient mutants both to validate our methods and repeat essential experiments performed by Daniels et al. (9). By site-directed mutagenesis of the genome of SV40 strain 776, we recreated the VP4-deficient mutant used in the original SV40-VP4 paper, SV40 VP2M228I. Due to the observed differences in infectivity between the two BKPyV VP4-deficient mutants, we also created SV40 VP2M228A. Due to the diversity in the biology of different cells (32), we used three different cell lines: BS-C-1, which was used in the original SV40-VP4 report, CV-1 cells, and Vero cells. Cells were transfected with equal amounts of WT SV40 or the two VP4-deficient mutants, and supernatants were harvested at 1, 2, and 4 dpt. In addition, supernatants from BS-C-1 cells were harvested at 5 dpt, since this time point was described in the original report as the time with the highest VP4 expression. An SV40-specific qPCR of DNase I-treated supernatants revealed that transfection of SV40 WT DNA in BS-C-1 cells gave an approximately 1-log increase in encapsidated viral genomes from 1 dpt to 2 dpt, an additional 1-log increase from 2 dpt to 4 dpt, and only a 0.5-log increase from 4 dpt to 5 dpt (Fig. 4A). Similarly, as observed for BKPyV VP4-deficient mutants, the SV40 VP4-deficient mutants were released at the same levels as the SV40 WT (Fig. 2B and 4A). In addition, when CV-1 cells or Vero cells were transfected, the SV40 VP4-deficient mutants were released at levels similar to the SV40 WT (Fig. 4A and data not shown). Of note, the amount of viral encapsidated genomes released from CV-1 cells and Vero cells at 2 dpt was approximately 1 log higher than that from BS-C-1 cells, suggesting either a more efficient transfection or a faster replication cycle than that in BS-C-1 cells.

The release of virions was also investigated by transfection of CV-1 cells followed by ultracentrifugation of supernatants harvested at 2 dpt, SDS-PAGE, and Western blotting of the pelleted virions. Based on the VP1, VP2, and VP3 bands, the result again confirmed a similar amount of released extracellular virus for the WT and VP4-deficient mutants (Fig. 4B). In agreement with observations by Daniels et al. (9), VP4 was not detected. We concluded that encapsidated genomes of the WT and the mutants were released at similar levels from transfected BS-C-1, CV-1, and Vero cells. Moreover, for BS-C-1 cells the majority of the progeny was already released at 4 dpt.

The BKPyV VP4-deficient mutants seemed to be inhibited in one or more early steps in the replication cycle prior to the DNA replication step (Fig. 2B, C, and D). To investigate if this was also the case for SV40 VP4-deficient mutants, we examined the infectivity of the SV40 progeny in CV-1 cells. Supernatants harvested from CV-1 cells at 2 dpt, containing progeny of either SV40 WT or the VP4-deficient mutants VP2M228A and VP2M228I, were used to infect new CV-1 cells. At 2 dpi, the cells were fixed and stained for LTag and VP1. Immunofluorescence microscopy revealed that infection with supernatants from three independent SV40 WT transfections resulted in between 14.3 and 25.2% LTag-expressing cells, i.e., infected cells. The percentage of cells with detectable VP1 staining ranged from 4.5 to 9.4%. Compared to supernatants from SV40 WT-transfected cells, supernatants from SV40 VP2M228I-transfected cells were less successful at infecting new CV-1 cells. The reduction was 43% and 57% for LTag and VP1, respectively (Fig. 4C). Interestingly, and in accordance with the results from BKPyV experiments (Fig. 2D), the SV40 VP2M228A mutation was better tolerated by the virus and resulted in an insignificant decrease of CV-1 infected cells (Fig. 4C).

We next wanted to investigate the expression of SV40 VP4 during infection of CV-1 cells. CV-1 cells were infected with the WT or the VP2M228I or VP2M228A mutant. At 72 hpi, the cells were harvested and separated into cytoplasmic and nuclear fractions before SDS-PAGE and Western blotting with the SV40 VP2/3 antiserum was performed. Cytoplasmic and nuclear fractions from mock-infected cells were used as controls. As expected, a strong expression of proteins with the predicted size of VP2 and VP3 was observed in nuclear extracts from WT-infected cells (Fig. 4D). As observed for BKPyV (Fig. 1E), a slightly faster migrating band was observed below VP2 and VP3. In addition, VP2 and VP3 were found in the cytoplasmic fractions, with some of them possibly originating from the virus inoculation. The pattern was the same for VP2M228I and VP2M228A but all bands were weaker for VP2M228I, supporting the earlier suggested reduced infectivity. Of note, a weak band between 8 and 15 kDa was seen for both WT and VP4-deficient mutants but was stronger in cytoplasmic than in nuclear fractions. Importantly, this band was also observed in fractions of mock-infected cells. As observed with fractions from RPTECs (Fig. 1E), several bands with molecular masses greater than 38 kDa were observed for both mock-infected and SV40-infected cells, possibly due to unspecific binding of the VP2/3 antiserum.

We conclude that SV40 does not need VP4 for an efficient release of progeny from BS-C-1 cells, CV-1 cells, or Vero cells. Of note, this is in disagreement with the conclusions made in the original SV40 VP4 report. Similar to what we observed for BKPyV, a methionine-to-isoleucine mutation in VP2 amino acid 228 and/or VP3 amino acid 110 reduces the infectious potential of SV40; however, for SV40 a methionine-to-alanine mutation is well tolerated. Western blotting of nuclear and cytoplasmic fractions from SV40-infected cells using the VP2/3 antisera revealed a band of size similar to that of VP4, but since this band was found in fractions from VP4-deficient mutants and mock-infected cells, this is unlikely to be VP4 and seems to be a cellular protein.

SV40 VP4 is not detected upon immunoprecipitation using SV40 VP2/3 antiserum or directly from nuclear extracts by MS analysis. As shown in Fig. 4D, we did detected a protein between 8 and 15 kDa in nuclear extract from SV40 WT-infected CV-1 cells by Western blotting with the SV40 VP2/3 antisera. In order to possibly detect VP4, we used LC-MS/MS. We first performed immunoprecipitation of the nuclear extract using the SV40 VP2/3 antisera. Nuclear extracts from SV40 WT-infected CV-1 cells were harvested when most of the cells displayed cytopathic effect (3 to 6 dpi), i.e., when expression of the putative very late VP4 protein presumably would be at its maximum. Western blotting of the immunoprecipitated proteins showed strong VP3 and VP2 bands

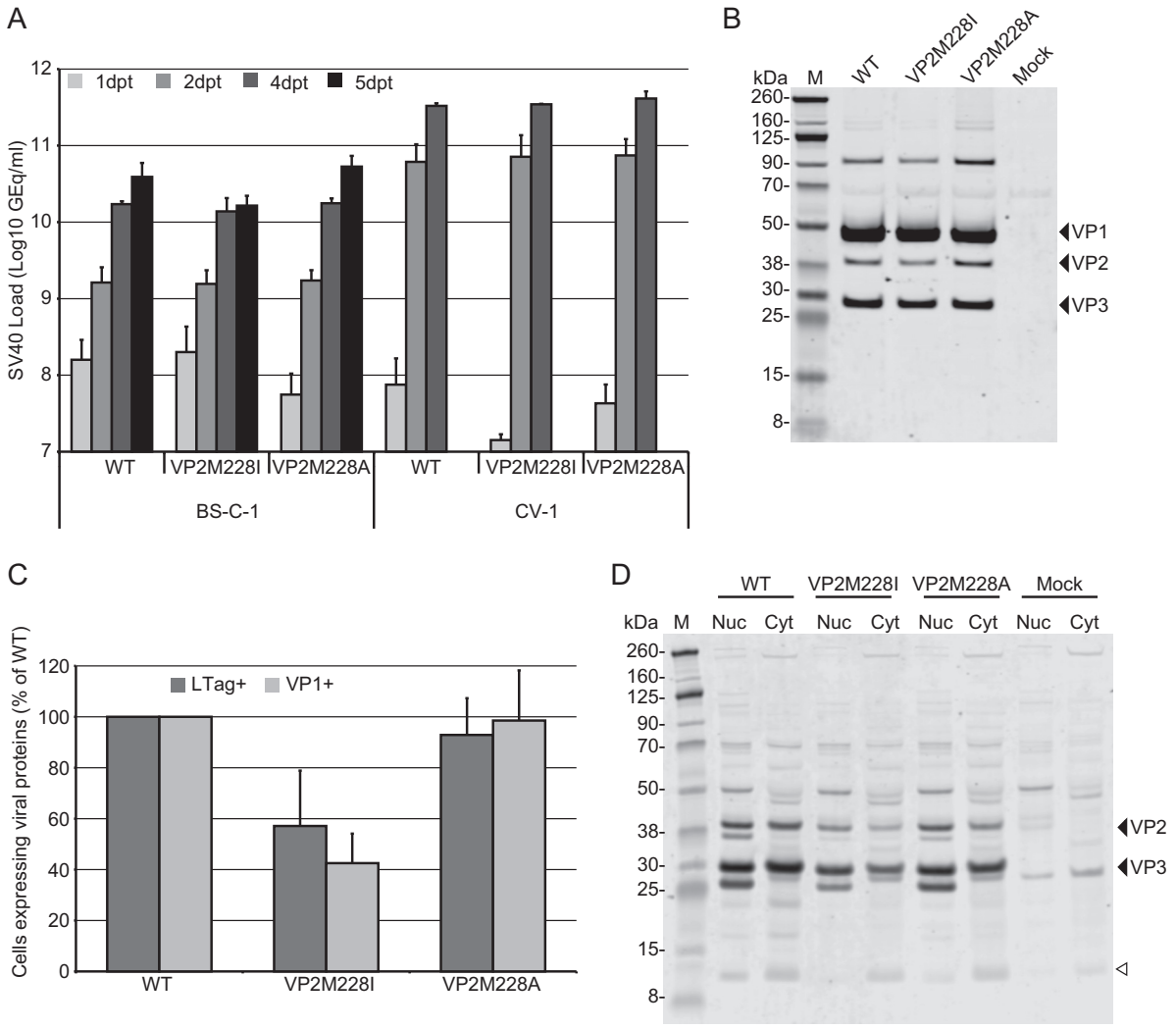

FIG 4 SV40 VP4 is not required for viral progeny release, but the VP4 start codon substitution affects infectivity. (A) SV40 load in DNase I-treated supernatants from BS-C-1 cells and CV-1 cells at 1, 2, 4, and 5 dpt, determined by real-time quantitative PCR and presented as GEq/ml. The figure represents data from three independent experiments (except BS-C-1 cells at 5 dpt and CV-1 cells at 4 dpt, which were performed twice). Each experiment was performed in duplicate wells, and the error bars indicate the standard deviations. (B) Western blot of capsid proteins pelleted by ultracentrifugation of CV-1 cell supernatants harvested 2 dpt. A volume corresponding to 400 μl supernatant was loaded on the gel. The membrane was probed with SV40 VP1 and VP2/3 antisera. (C) Quantification of infectivity in CV-1 cells at 2 dpi with SV40 WT and VP4-deficient mutants. CV-1 cells were infected with the indicated SV40 variants at similar viral load (approximately 10 $\log_{10}$ GEq/ml). Quantification of LTag- and VP1-positive cells in relation to the SV40 WT infection, determined by immunofluorescence microscopy, is displayed in the graph. Immunofluorescence staining was performed using the SV40 VP1 antisera and the LTag antibody (Pab419), and the quantification is related to the number of SV40 WT-infected cells. Each experiment was done in duplicate and repeated twice. Approximately 3,000 to 5,000 Draq5-positive cells per well were analyzed for virus protein expression. (D) Western blot of nuclear and cytoplasmic fractions from CV-1 cells that were mock infected or SV40 infected with the indicated SV40 variants and harvested at 2 dpi. The membrane was probed with SV40 VP2/3 antisera. The empty arrowhead indicates a band with a size similar to that of the putative VP4 protein. Nuc, nuclear fraction; Cyt, cytoplasmic fraction; M, molecular mass marker.

and some weaker faster-migrating bands about the size of VP4 (Fig. 5A). In Coomassie-stained SDS-PAGE gels, visible bands below 20 kDa were subjected to in-gel trypsin digestion and LC-MS/MS. In addition to some cellular proteins (data not shown), we were able to detect three viral peptides. While two were derived from VP2 and/or VP3, one of them could be derived from VP4 (Fig. 5B). However, due to the common C terminus of VP2/3/4, it could also be derived from the two minor capsid proteins. None of the peptides could originate from the putative VP5.

Two bands corresponding to the size of VP2 were also visible and were identified by LC-MS/MS as originating from VP2. VP3 was not clearly seen on Coomassie-stained gel, as VP3 comigrates with the IgG light chains deriving from the antibodies used in the immunoprecipitation. This experiment was repeated once with the same result.

Since the minor capsid proteins are known to be hydrophobic and thus might not be the ideal substrate for trypsin (33), the experiment was repeated using chymotrypsin instead of trypsin. Gel pieces from approximately 21 kDa to 6 kDa were excised (Fig. 5C), fragmented, and subjected to LC-MS/MS for identification. This time, peptides deriving from viral proteins were not detected in gel pieces below 21 kDa. From the gel piece excised close to 21.5 kDa, three viral peptides were detected, and one of them could belong to VP4. However, since it was excised high in the gel, it

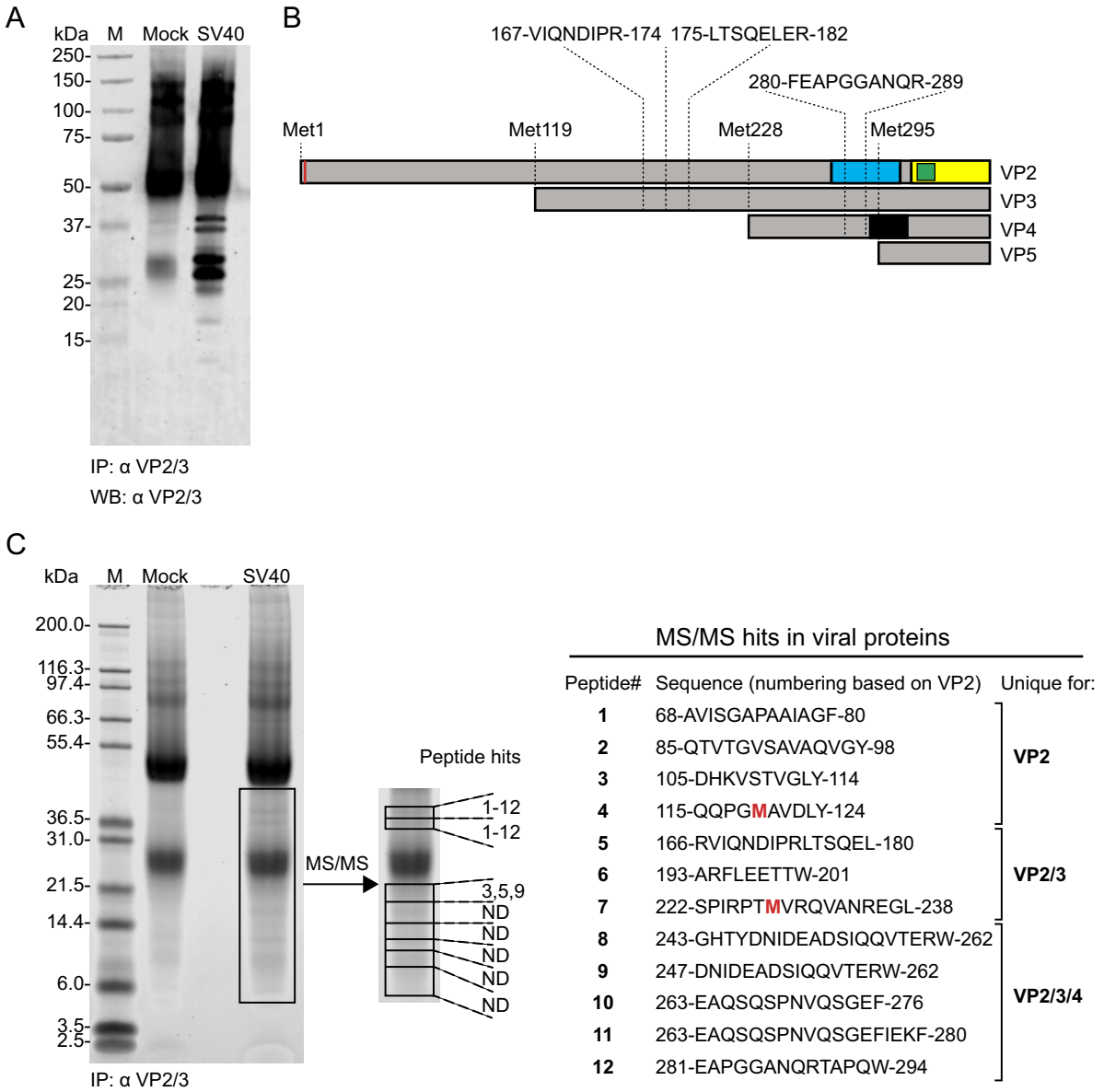

FIG 5 SV40 VP4 is not detected upon immunoprecipitation (IP) using SV40 VP2/3 antiserum. (A) Western blot (WB) of immunoprecipitated proteins from nuclear extracts of SV40-infected CV-1 cells at 6 dpi. Immunoprecipitation was performed using the SV40 VP2/3 antisera. The membrane was probed with SV40 VP2/3 antisera. M, molecular mass marker. (B) Schematic presentation of the location in VP2 of the peptides identified by LC-MS/MS from visible bands below 20 kDa excised from a Coomassie-stained SDS-PAGE gel after immunoprecipitation. Note that the SV40 VP5 ORF is similar to the BKPyV VP6 ORF, as shown in Fig. 1A. (C) Coomassie-stained SDS-PAGE gel of immunoprecipitated proteins from nuclear extracts of SV40-infected CV-1 cells at 6 dpi. The location of the excised bands and the sequence of VP2/3/4 peptides detected in these bands are listed. The initial methionine residues for both VP3 and VP4 are highlighted in red. The gel pieces were fragmented in gel by chymotrypsin. ND, not detected; M, molecular mass marker.

likely derived from degraded VP2 or VP3. We again excised the two bands that corresponded to VP2, and LC-MS/MS was able to identify 12 peptides deriving from VP2 (Fig. 5C), proving that chymotrypsin is suitable for fragmentation of VP2/3/4.

Since immunoprecipitation using the SV40 VP2/3 antiserum gave significant amounts of background and minimal concentrating effect, we attempted to detect SV40 VP4 directly from nuclear extracts of SV40-infected CV-1 cells by LC-MS/MS. By combining N-terminal dimethyl labeling at the protein level with LC-MS/MS, it is possible to identify the N-terminal part of a protein. Therefore, to be able to separate the N terminus of VP4 from VP2 or VP3 peptides, we performed dimethyl labeling of the N terminus in nuclear extracts from SV40-infected CV-1 cells. If VP4 is present in the sample, this labeling will give a VP4-specific peptide distinguishable from VP2/3-derived peptides. To create a positive control containing the dimethyl-labeled N-terminal VP4 peptide, we first transfected the SV40 VP4-eGFP expression vector into CV-1 cells (Fig. 1D) and subjected the nuclear extract at 1 dpt to dimethyl labeling. The fusion protein was used to determine the LC retention time of the N-terminal dimethyl-labeled chymotryptic peptide of VP4. In this sample, we identified two chymotryptic N-terminal peptides, VRQVANREGL and VRQVANREGLQISF,

both with dimethylated N-terminal valine. As evidenced by the missing N-terminal methionine and dimethylation at valine, the N-terminal methionine is removed by the host methionine aminopeptidase (34). In addition, other internal chymotryptic peptides were identified, leading to a 56% sequence coverage of the VP4 protein in the positive control.

In the sample from infected cells, two peptides that could originate from VP2, VP3, or VP4 were found, as well as one peptide originating from VP2 or VP3. However, careful examination of the raw data showed no trace of the possible N-terminal peptides of VP4. In addition, the major capsid protein VP1 was identified with a total of 7 chymotryptic peptides.

We conclude that there is no decisive evidence of VP4 in nuclear extracts from SV40-infected CV-1 cells upon immunoprecipitation with an SV40 VP3 antisera or by an unbiased approach using N-terminal dimethyl labeling.

The VP4-deficient mutant SV40 VP2M228A, but not SV40 VP2M228I, displays lytic properties similar to those of the SV40 WT strain. In the original VP4 report (9), trypan blue staining of infected BS-C-1 cells was used to demonstrate a 2-day delay in cell lysis caused by the VP4-deficient mutant SV40 VP2M228I (5 dpi) compared to SV40 WT (3 dpi).

Given the observed differences in infectivity between the two SV40 VP4-deficient mutants (Fig. 4C), we decided to compare the effect of the SV40 WT and VP4-deficient mutants on host cell viability in real time by the use of the xCELLigence system. This system utilizes electrode sensor arrays in the bottom of each well, emitting noninvasive electric signals, and measures changes in electrical impedance displayed as an arbitrary unit termed the cell index. Electrical impedance and, consequently, cell index, increases with increasing cell number, size, and attachment and thus gives an indication of the overall cell viability.

To ensure equal amounts of the different viruses, we initiated infection of CV-1 cells by DNA transfection. The transfection efficiency was low at approximately 10%. CV-1 cells were selected as the replication cycle seems quicker than that in BS-C-1 cells (Fig. 4A), allowing at least two replication cycles of SV40 WT to occur during the 5-day-long experiment. At about 6 hpt, cells were trypsinized and seeded into wells in the E-plate, and the 120 h of monitoring started. The cells transfected with an empty plasmid vector (mock) were proliferating throughout the experiment, giving a steady increase in cell index; therefore, the cell indexes of cells transfected with SV40 WT, VP2M228I, or VP2M228A were normalized to the cell index of mock-transfected cells (Fig. 6A). From about 48 hpt, a decline in the cell index of wells with virus-transfected cells was observed. Interestingly, the decline was equal for all SV40 variants and coincided in time with the approximately 3-log increase of released DNase I-protected virus DNA observed in Fig. 4A, suggesting that the decline was caused by lytic progeny release from the virus-transfected cells. Shortly before 90 hpt, the cell index of the wells with WT virus started to decline steeply and, with a few hours' delay, was followed by a decline in the cell index of the VP2M228A mutant. According to the experiment depicted in Fig. 4A, at 96 hpt, the virus DNA load is further increased by 1 log, which suggests that the latter decline was caused by lytic release of virions from cells infected by progeny virus during the experiment. By the end of the experiment at 120 hpt, the cell index in wells with the WT and the VP2M228A mutant was clearly different from those of the wells with mock-transfected cells and wells with the VP2M228I mutant. While both the WT virus and the VP2M228A mutant caused an ~6-U decline in cell index, the VP2M228I mutant caused only a ~2-U decline compared to mock-transfected cells. The remaining cells were fixed and stained for LTag (red), VP1 (green), and DNA (blue) (Fig. 6A). As indicated by the decline in cell index, the number of cells in wells transfected with the WT and VP2M228A mutant was severely reduced, supporting virus-induced lytic release. The number of cells in wells transfected with VP2M228I was also reduced compared to wells with mock-transfected cells but to a lesser degree, again in agreement with the cell index curve (Fig. 6A).

For a visual investigation of the lytic properties of the SV40 WT and the VP4-deficient mutants over time, real-time microscopy of CV-1-infected cells in the presence of a DNA stain staining only dead cells was used. In short, CV-1 cells were infected by CV-1 supernatants harvested at 2 dpt, the green cyanine dye was added, and photographs were taken every 15 min up to 5 dpi. While cells infected with the WT or the VP2M228A mutant started to die from 2 dpi, initial cell death in VP2M228I-infected cells was delayed by about 1 day (Fig. 6B; also see Movies S1 to S4 in the supplemental material). At the end of the experiment 5 dpi, immunofluorescence staining was performed. VP1 staining revealed fewer infected cells, and the phase contrast showed a more confluent cell layer for the VP2M228I-infected cells than for WT- and VP2M228A-infected cells (Fig. 6C).

We conclude that the virus-induced cell death is not dependent on VP4. Since the progeny mainly from WT- and VP2M228A-transfected cells seemed to efficiently initiate a lytic infection of new cells, methionine in position 228 in VP2 and/or position 110 in VP3 seems to be required for optimal viral fitness.

DISCUSSION

Several steps in the replication cycle of polyomaviruses remain enigmatic despite several decades of investigation. Among the least-studied steps is viral egress. As for other nonenveloped viruses, viral egress earlier was thought to exclusively occur passively by host cell lysis. A decade ago, however, this concept was challenged in the case of polyomaviruses, as it was reported that the newly discovered SV40 VP4, possibly in collaboration with the minor capsid proteins VP2/3, act as a viroporin triggering host cell lysis in a more active and timely manner. Here, we show that VP4 is not required for release of BKPyV from RPTECs. More surprisingly, and contradicting the previous report, VP4 is not required for efficient release of SV40 from various permissive cell types, including BS-C-1. Despite several attempts, we were not able to detect SV40 VP4 in SV40-infected cells by mass spectroscopy.

Due to the reported finding of VP4 in SV40, we sought to investigate if we could detect VP4 in BKPyV-infected RPTECs. The antiserum raised against SV40 VP3 was found to recognize recombinant BKPyV eGFP-VP4 fusion proteins (Fig. 1B and C), and we were able to detect a couple of faint bands between 10 and 15 kDa when this antibody was used for Western blot analysis of nuclear extracts from BKPyV-infected RPTECs (Fig. 1E). However, it is apparent that the SV40 VP2/3 antiserum recognizes a range of cellular proteins, including a faint band between 8 and 15 kDa in the mock-infected RPTECs as well as in CV-1 cells (Fig. 4D), raising the possibility that a cellular protein could have been misidentified as VP4 in the original paper.

Surprisingly, transfection experiments using BKPyV and SV40 VP4-deficient mutants, as well as BKPyV deficient in one or both minor capsid proteins, showed that all mutants were capable of

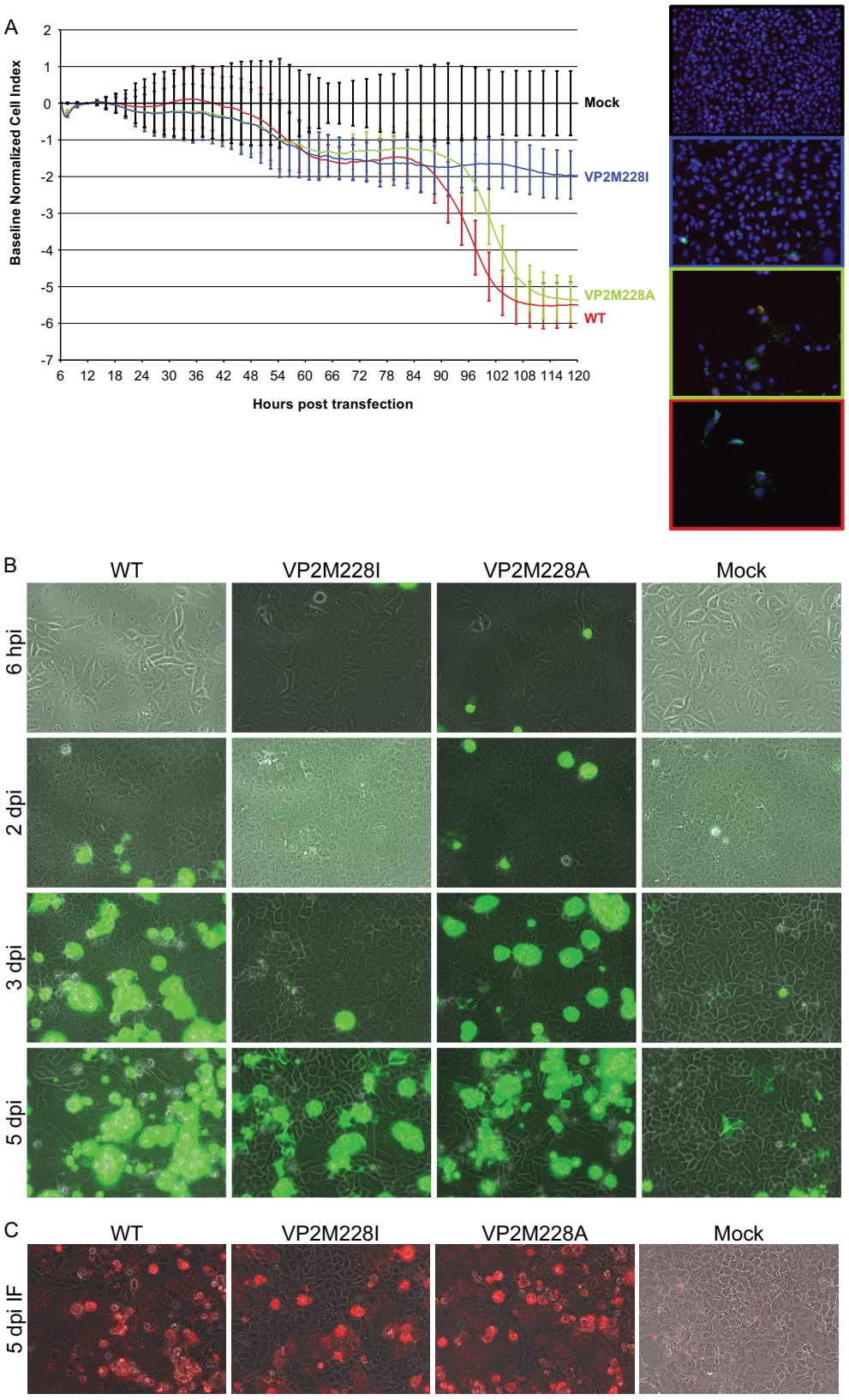

FIG 6 SV40 VP2M228I shows a delayed and reduced host cell lysis compared to WT SV40. (A) Electrical impedance in SV40-transfected CV-1 monolayers was measured using the xCELLigence system from 6 to ~120 hpt. The cell index was normalized to the cell index of mock-transfected cells. The experiment was repeated 2 times, and a representative experiment where the cell index of 4 parallel wells was measured and shown as means with standard deviations is presented. At the end of this experiment, immunofluorescence staining was performed using the SV40 VP1 antisera (green), an LTag antibody (Pab419; red), and the DNA stain Draq5 (blue). (B) Time-lapse microscopy was used to monitor SV40-infected CV-1 monolayers from 6 hpi until 120 hpi (5 dpi). A green cyanine dye staining the DNA of dead cells green was added directly after infection. Photos were taken every 15 min, and selected time points (6 hpi, 2 dpi, 3 dpi, and 5 dpi) are shown. (C) Immunofluorescence staining of SV40-infected CV-1 cells at the end of the time-lapse experiment described for panel B, using the SV40 VP1 antisera (red). A Nikon Biostation was used to take immunofluorescence and phase contrast images, and merged images are shown.

releasing virions at levels similar to that of the WT strains (Fig. 2B and C and 4A and B). However, the infectivity of the BKPyV mutants deficient for either VP2, VP3, VP4, or both VP2 and VP3 was strongly reduced. Similar results were found for the SV40 VP4-deficient mutant VP2M228I, while the VP2M228A mutant was still infectious (Fig. 2D and 4C).

The fact that the VP4-deficient mutants of both BKPyV and SV40 all were able to produce and release progeny viruses upon DNA transfection of several relevant susceptible cells rules out that VP4 has a role in viral progeny release, at least in cell culture. In addition, the lack of VP4 in the viral particle (Fig. 4B) excludes a role in viral entry. It is obvious, however, that the infectivity of the VP4-deficient mutants is reduced. The mutation of one amino acid in BKPyV VP2 (amino acid 229) and/or BKPyV VP3 (amino acid 110), and likewise one amino acid in SV40 VP2 (amino acid 228) and/or SV40 VP3 (amino acid 110), seems to negatively affect the viral replication cycle at a stage prior to viral DNA replication, as the effect is not noticed upon DNA transfection. Alteration of methionine to isoleucine is less tolerated than alteration to alanine, and the noticed difference in infectivity between the different mutants supports that the effect is due to alteration in VP2 or VP3 rather than the loss of the VP4 ORF. This methionine is a part of a conserved motif (MVRQVA) in the VP2/3 proteins found in about 20% of human and nonhuman primate polyomaviruses (35, 36).

When Daniels et al. (9) infected BS-C-1 cells with SV40 WT and the VP4-deficient SV40 VP2M228I mutant, they observed a significant decrease in the infectivity and host cell lysis for the latter and attributed this to the mutant's defect in lytic release. Also in a recent paper from an independent group investigating SV40 virus protein involvement in vacuolization, a deficient release of infectious virus particles for the SV40 VP2M228I mutant was concluded (37). In our opinion, both of these studies used inadequate methods to characterize the release of the mutants. We applied methods involving transfection, which bypasses the viral entry stage, quantitative PCR of DNase I protected viral DNA in supernatants, and Western blotting of released virus, and this revealed similar levels of extracellular viral DNA and proteins for all mutants. However, when infecting naive cells with similar titers of virus, as quantified by qPCR, the infectivity of VP4-deficient mutants was clearly reduced. This indicates a high ratio of viral DNA to infectious particle compared to that for the WT. Hence, we suggest that the reduction in the infectivity of the VP4-deficient mutant seen by us, Daniels et al. (9), and Luo et al. (37) is indeed due to a defect in entry events and not to release of the mutants.

Interestingly, the VP4-deficient SV40 mutant VP2M228I was recognized by Tange et al. (38) to be identical to that of the SV40 temperature-sensitive D-type mutant, tsD222. This class of temperature-sensitive mutants exhibit, at the restrictive temperature of 40°C, an apparent defect in the uncoating process, as shown by a failure to initiate viral replication (39). The viral DNA of these mutants were, however, able to initiate infection similar to that of the WT upon DNA transfection (40, 41). Tange and coworkers were not able to reproduce the Western blot results from the original VP4 report even when using SV40 VP2/3 antibodies from the same source. Apparently, they frequently detected proteins of approximately 25, 18, 16, and 12 kDa deriving from VP2/3. By doing complementation experiments, Tange and colleagues concluded that the growth defect of the tsD222 mutant was not due to the lack of VP4-ORF (38) and thus support our conclusions.

Mutating the start codons of the BKPyV minor capsid proteins alone or together reduced infectivity by over 99% compared to the WT. As far as we know, this is the first time this has been demonstrated for BKPyV, but it is in agreement with experiments done with BKPyV pseudoviruses or mouse polyomavirus, SV40, and JCPyV mutants deficient in either VP2 or VP3 or both VP2 and VP3 (42–46). Based on our results, we conclude that VP2 is crucial in early events of a BKPyV infection in RPTECs. The same seems to be true for VP3, but there is a possibility that the observed difference for the VP3-deficient mutant is an effect of the mutation introduced in amino acid position 120 in VP2. To investigate this, one could make other VP3-deficient mutants by replacing this methionine in VP2 with less bulky amino acids. Although the entry of BKPyV and SV40 into host cells is not fully understood, SV40 VP2 in particular seems to play essential roles in the transport of the partly dissembled particles from the endoplasmic reticulum (ER) to the cytosol (47–49), while both VP2 and VP3 for both SV40 and BKPyV are important for the nuclear import of the viral genomes (50, 51). So far, we do not know which of these steps are disrupted during infection with our mutants.

Attempts to conclusively identify VP4 in nuclear extracts from SV40-infected CV-1 cells using LC-MS/MS failed. By immunoprecipitation using the SV40 VP2/3 antiserum, we were able to detect peptides that could originate from VP2, VP3, or VP4, but detection of VP2 and VP3 peptides in samples that migrated below 20 kDa on SDS-PAGE indicated that VP2 and VP3 are prone to degradation or proteolysis (Fig. 1C). This has also been observed by Tange et al. (38). Similar results were obtained when LC-MS/MS was performed directly on nuclear extracts from SV40-infected cells CV-1 following N-terminal dimethyl labeling.

Based on our results, we believe that BKPyV and SV40 progeny is released from host cells by a mechanism not depending on a VP4 viroporin. While Movies S1 to 4 in the supplemental material and Fig. 6B suggest that SV40 is released by a lytic mechanism, strong cytopathic effects are rarely seen in BKPyV-infected cells. Interestingly, a nonlytic directional release of SV40 from polarized primary African green monkey cells and Vero cells and a nonlytic release of BKPyV from RPTECs has been reported (52, 53). Recently nonlytic release has been demonstrated for several nonenveloped viruses, such as poliovirus, hepatitis A virus (HAV), parvovirus, and hepatitis E virus (reviewed in references 54 and 55). These viruses seem to utilize autophagy or similar pathways to release viral progeny enclosed in membranes without killing the host cell, and the viral particles seem to be infectious with or without the membrane. So far, there is no evidence for release of polyomavirus enclosed in membranes, but it is possible that SV40 and BKPyV can use both a lytic and a nonlytic pathway for release.

In conclusion, neither BKPyV nor SV40 requires VP4 for progeny release from their natural host cells, but one conserved methionine in VP2 seems important for viral replication, probably influencing viral entry or uncoating. Moreover, BKPyV needs both VP2 and VP3 to form infectious viral particles.

ACKNOWLEDGMENTS

We thank Garth D. Tylden at the Department of Microbiology and Infection Control at the University Hospital of North Norway for helpful discussions and critical reading of the manuscript and Toril Anne Grønset at

the Tromsø University Proteomics Platform for help with the mass spectrometry analysis.

We have no conflicts of interest to declare.

FUNDING INFORMATION

This work, including the efforts of Stian Henriksen and Christine Hanssen Rinaldo, was funded by the University Hospital of North Norway.

The funders had no role in study design, data collection and interpretation, or the decision to submit the work for publication.

REFERENCES

1. **Drachenberg CB, Papadimitriou JC, Wali R, Cubitt CL, Ramos E.** 2003. BK polyoma virus allograft nephropathy: ultrastructural features from viral cell entry to lysis. Am J Transplant **3:**1383–1392. http://dx.doi.org/10.1046/j.1600-6135.2003.00237.x.
2. **Hirsch HH.** 2010. Polyoma and papilloma virus infections after hematopoietic stem cell or solid organ transplantation, p 465–482. *In* Bowden P, Ljungman P, Snydman DR (ed), Transplant infections, 3rd ed. Lippincott Williams & Wilkins, Philadelphia, PA.
3. **Hirsch HH, Kardas P, Kranz D, Leboeuf C.** 2013. The human JC polyomavirus (JCPyV): virological background and clinical implications. APMIS **121:**685–727. http://dx.doi.org/10.1111/apm.12128.
4. **Mazlo M, Tariska I.** 1980. Morphological demonstration of the first phase of polyomavirus replication in oligodendroglia cells of human brain in progressive multifocal leukoencephalopathy (PML). Acta Neuropathol **49:**133–143. http://dx.doi.org/10.1007/BF00690753.
5. **Liddington RC, Yan Y, Moulai J, Sahli R, Benjamin TL, Harrison SC.** 1991. Structure of simian virus 40 at 3.8-A resolution. Nature **354:**278–284. http://dx.doi.org/10.1038/354278a0.
6. **Stehle T, Gamblin SJ, Yan Y, Harrison SC.** 1996. The structure of simian virus 40 refined at 3.1 A resolution. Structure **4:**165–182. http://dx.doi.org/10.1016/S0969-2126(96)00020-2.
7. **Griffith JP, Griffith DL, Rayment I, Murakami WT, Caspar DL.** 1992. Inside polyomavirus at 25-A resolution. Nature **355:**652–654. http://dx.doi.org/10.1038/355652a0.
8. **Rinaldo CH, Tylden GD, Sharma BN.** 2013. The human polyomavirus BK (BKPyV): virological background and clinical implications. APMIS **121:**728–745. http://dx.doi.org/10.1111/apm.12134.
9. **Daniels R, Sadowicz D, Hebert DN.** 2007. A very late viral protein triggers the lytic release of SV40. PLoS Pathog **3:**e98. http://dx.doi.org/10.1371/journal.ppat.0030098.
10. **Gosert R, Rinaldo CH, Funk GA, Egli A, Ramos E, Drachenberg CB, Hirsch HH.** 2008. Polyomavirus BK with rearranged noncoding control region emerge in vivo in renal transplant patients and increase viral replication and cytopathology. J Exp Med **205:**841–852. http://dx.doi.org/10.1084/jem.20072097.
11. **Olsen GH, Hirsch HH, Rinaldo CH.** 2009. Functional analysis of polyomavirus BK non-coding control region quasispecies from kidney transplant recipients. J Med Virol **81:**1959–1967. http://dx.doi.org/10.1002/jmv.21605.
12. **Nieva JL, Madan V, Carrasco L.** 2012. Viroporins: structure and biological functions. Nat Rev Microbiol **10:**563–574. http://dx.doi.org/10.1038/nrmicro2820.
13. **Suzuki T, Orba Y, Okada Y, Sunden Y, Kimura T, Tanaka S, Nagashima K, Hall WW, Sawa H.** 2010. The human polyoma JC virus agnoprotein acts as a viroporin. PLoS Pathog **6:**e1000801. http://dx.doi.org/10.1371/journal.ppat.1000801.
14. **Giorda KM, Raghava S, Zhang MW, Hebert DN.** 2013. The viroporin activity of the minor structural proteins VP2 and VP3 is required for SV40 propagation. J Biol Chem **288:**2510–2520. http://dx.doi.org/10.1074/jbc.M112.428425.
15. **Raghava S, Giorda KM, Romano FB, Heuck AP, Hebert DN.** 2011. The SV40 late protein VP4 is a viroporin that forms pores to disrupt membranes for viral release. PLoS Pathog **7:**e1002116. http://dx.doi.org/10.1371/journal.ppat.1002116.
16. **Raghava S, Giorda KM, Romano FB, Heuck AP, Hebert DN.** 2013. SV40 late protein VP4 forms toroidal pores to disrupt membranes for viral release. Biochemistry **52:**3939–3948. http://dx.doi.org/10.1021/bi400036z.
17. **Giorda KM, Raghava S, Hebert DN.** 2012. The Simian virus 40 late viral protein VP4 disrupts the nuclear envelope for viral release. J Virol **86:**3180–3192. http://dx.doi.org/10.1128/JVI.07047-11.
18. **Henriksen S, Mittelholzer C, Gosert R, Hirsch HH, Rinaldo CH.** 2015. Human BK polyomavirus plasmid pBKV (34-2) (Dunlop) contains mutations not found in the originally published sequences. Genome Announc **3:**00046-15.
19. **Johnsen JI, Seternes OM, Johansen T, Moens U, Mantyjarvi R, Traavik T.** 1995. Subpopulations of non-coding control region variants within a cell culture-passaged stock of BK virus: sequence comparisons and biological characteristics. J Gen Virol **76:**1571–1581. http://dx.doi.org/10.1099/0022-1317-76-7-1571.
20. **Lednicky J, Folk WR.** 1992. Two synthetic Sp1-binding sites functionally substitute for the 21-base-pair repeat region to activate simian virus 40 growth in CV-1 cells. J Virol **66:**6379–6390.
21. **Henriksen S, Tylden GD, Dumoulin A, Sharma BN, Hirsch HH, Rinaldo CH.** 2014. The human fetal glial cell line SVG p12 contains infectious BK polyomavirus (BKPyV). J Virol **88:**7556–7568. http://dx.doi.org/10.1128/JVI.00696-14.
22. **Lamark T, Perander M, Outzen H, Kristiansen K, Overvatn A, Michaelsen E, Bjorkoy G, Johansen T.** 2003. Interaction codes within the family of mammalian Phox and Bem1p domain-containing proteins. J Biol Chem **278:**34568–34581. http://dx.doi.org/10.1074/jbc.M303221200.
23. **Rinaldo CH, Gosert R, Bernhoff E, Finstad S, Hirsch HH.** 2010. 1-O-hexadecyloxypropyl cidofovir (CMX001) effectively inhibits polyomavirus BK replication in primary human renal tubular epithelial cells. Antimicrob Agents Chemother **54:**4714–4722. http://dx.doi.org/10.1128/AAC.00974-10.
24. **Rinaldo CH, Traavik T, Hey A.** 1998. The agnogene of the human polyomavirus BK is expressed. J Virol **72:**6233–6236.
25. **Rinaldo CH, Myhre MR, Alstad H, Nilssen O, Traavik T.** 2003. Human polyomavirus BK (BKV) transiently transforms and persistently infects cultured osteosarcoma cells. Virus Res **93:**181–187. http://dx.doi.org/10.1016/S0168-1702(03)00096-0.
26. **Dumoulin A, Hirsch HH.** 2011. Reevaluating and optimizing polyomavirus BK and JC real-time PCR assays to detect rare sequence polymorphisms. J Clin Microbiol **49:**1382–1388. http://dx.doi.org/10.1128/JCM.02008-10.
27. **Li RM, Mannon RB, Kleiner D, Tsokos M, Bynum M, Kirk AD, Kopp JB.** 2002. BK virus and SV40 co-infection in polyomavirus nephropathy. Transplantation **74:**1497–1504. http://dx.doi.org/10.1097/00007890-200212150-00004.
28. **Jentoft N, Dearborn DG.** 1979. Labeling of proteins by reductive methylation using sodium cyanoborohydride. J Biol Chem **254:**4359–4365.
29. **Shevchenko A, Wilm M, Vorm O, Mann M.** 1996. Mass spectrometric sequencing of proteins silver-stained polyacrylamide gels. Anal Chem **68:**850–858. http://dx.doi.org/10.1021/ac950914h.
30. **Low J, Humes HD, Szczypka M, Imperiale M.** 2004. BKV and SV40 infection of human kidney tubular epithelial cells in vitro. Virology **323:**182–188. http://dx.doi.org/10.1016/j.virol.2004.03.027.
31. **Bernhoff E, Gutteberg TJ, Sandvik K, Hirsch HH, Rinaldo CH.** 2008. Cidofovir inhibits polyomavirus BK replication in human renal tubular cells downstream of viral early gene expression. Am J Transplant **8:**1413–1422. http://dx.doi.org/10.1111/j.1600-6143.2008.02269.x.
32. **Bennett SM, Jiang M, Imperiale MJ.** 2013. Role of cell-type-specific endoplasmic reticulum-associated degradation in polyomavirus trafficking. J Virol **87:**8843–8852. http://dx.doi.org/10.1128/JVI.00664-13.
33. **Tsiatsiani L, Heck AJ.** 2015. Proteomics beyond trypsin. FEBS J **282:**2612–2626.
34. **Bradshaw RA, Brickey WW, Walker KW.** 1998. N-terminal processing: the methionine aminopeptidase and N alpha-acetyl transferase families. Trends Biochem Sci **23:**263–267. http://dx.doi.org/10.1016/S0968-0004(98)01227-4.
35. **Van Ghelue M, Khan MT, Ehlers B, Moens U.** 2012. Genome analysis of the new human polyomaviruses. Rev Med Virol **22:**354–377. http://dx.doi.org/10.1002/rmv.1711.
36. **Ehlers B, Moens U.** 2014. Genome analysis of non-human primate polyomaviruses. Infect Genet Evol **26:**283–294. http://dx.doi.org/10.1016/j.meegid.2014.05.030.
37. **Luo Y, Motamedi N, Magaldi TG, Gee GV, Atwood WJ, DiMaio D.** 2016. Interaction between simian virus 40 major capsid protein VP1 and cell surface ganglioside GM1 triggers vacuole formation. mBio **7**(2):e00297.
38. **Tange S, Imai T, Nakanishi A.** 2011. An SV40 mutant defective in VP4 expression exhibits a temperature-sensitive growth defect. Virus Res **157:**116–120. http://dx.doi.org/10.1016/j.virusres.2011.02.001.

39. **Chou JY, Avila J, Martin RG.** 1974. Viral DNA synthesis in cells infected by temperature-sensitive mutants of simian virus 40. J Virol **14:**116–124.
40. **Robb JA, Martin RG.** 1972. Genetic analysis of simian virus 40. 3. Characterization of a temperature-sensitive mutant blocked at an early stage of productive infection in monkey cells. J Virol **9:**956–968.
41. **Avila J, Saral R, Martin RG, Khoury G.** 1976. The temperature-sensitive defect in SV40 group D mutants. Virology **73:**89–95. http://dx.doi.org/10.1016/0042-6822(76)90063-5.
42. **Schowalter RM, Reinhold WC, Buck CB.** 2012. Entry tropism of BK and Merkel cell polyomaviruses in cell culture. PLoS One **7:**e42181. http://dx.doi.org/10.1371/journal.pone.0042181.
43. **Mannova P, Liebl D, Krauzewicz N, Fejtova A, Stokrova J, Palkova Z, Griffin BE, Forstova J.** 2002. Analysis of mouse polyomavirus mutants with lesions in the minor capsid proteins. J Gen Virol **83:**2309–2319. http://dx.doi.org/10.1099/0022-1317-83-9-2309.
44. **Daniels R, Rusan NM, Wadsworth P, Hebert DN.** 2006. SV40 VP2 and VP3 insertion into ER membranes is controlled by the capsid protein VP1: implications for DNA translocation out of the ER. Mol Cell **24:**955–966. http://dx.doi.org/10.1016/j.molcel.2006.11.001.
45. **Gasparovic ML, Gee GV, Atwood WJ.** 2006. JC virus minor capsid proteins Vp2 and Vp3 are essential for virus propagation. J Virol **80:**10858–10861. http://dx.doi.org/10.1128/JVI.01298-06.
46. **Bagchi P, Walczak CP, Tsai B.** 2015. The endoplasmic reticulum membrane J protein C18 executes a distinct role in promoting simian virus 40 membrane penetration. J Virol **89:**4058–4068. http://dx.doi.org/10.1128/JVI.03574-14.
47. **Geiger R, Andritschke D, Friebe S, Herzog F, Luisoni S, Heger T, Helenius A.** 2011. BAP31 and BiP are essential for dislocation of SV40 from the endoplasmic reticulum to the cytosol. Nat Cell Biol **13:**1305–1314. http://dx.doi.org/10.1038/ncb2339.
48. **Goodwin EC, Lipovsky A, Inoue T, Magaldi TG, Edwards AP, Van Goor KE, Paton AW, Paton JC, Atwood WJ, Tsai B, DiMaio D.** 2011. BiP and multiple DNAJ molecular chaperones in the endoplasmic reticulum are required for efficient simian virus 40 infection. mBio **2:**e00101-11. http://dx.doi.org/10.1128/mBio.00101-11.
49. **Ravindran MS, Bagchi P, Cunningham CN, Tsai B.** 2016. Opportunistic intruders: how viruses orchestrate ER functions to infect cells. Nat Rev Microbiol **14:**407–420. http://dx.doi.org/10.1038/nrmicro.2016.60.
50. **Nakanishi A, Shum D, Morioka H, Otsuka E, Kasamatsu H.** 2002. Interaction of the Vp3 nuclear localization signal with the importin alpha 2/beta heterodimer directs nuclear entry of infecting simian virus 40. J Virol **76:**9368–9377. http://dx.doi.org/10.1128/JVI.76.18.9368-9377.2002.
51. **Bennett SM, Zhao L, Bosard C, Imperiale MJ.** 2015. Role of a nuclear localization signal on the minor capsid proteins VP2 and VP3 in BKPyV nuclear entry. Virology **474:**110–116. http://dx.doi.org/10.1016/j.virol.2014.10.013.
52. **Clayson ET, Brando LV, Compans RW.** 1989. Release of simian virus 40 virions from epithelial cells is polarized and occurs without cell lysis. J Virol **63:**2278–2288.
53. **Evans GL, Caller LG, Foster V, Crump CM.** 2015. Anion homeostasis is important for non-lytic release of BK polyomavirus from infected cells. Open Biol **5:**150041. http://dx.doi.org/10.1098/rsob.150041.
54. **Bird SW, Kirkegaard K.** 2015. Escape of non-enveloped virus from intact cells. Virology **479-480:**444–449.
55. **Bar S, Rommelaere J, Nuesch JP.** 2013. Vesicular transport of progeny parvovirus particles through ER and Golgi regulates maturation and cytolysis. PLoS Pathog **9:**e1003605. http://dx.doi.org/10.1371/journal.ppat.1003605.